34th Annual International Conference of the IEEE EMBS
San Diego, California USA, 28 August - 1 September, 2012

An Improved Ultra Wideband Channel Model Including the Frequency-Dependent Attenuation for In-Body Communications

A. Khaleghi, R. Chávez-Santiago, and I. Balasingham, *Senior Member, IEEE*

Abstract— **Ultra wideband (UWB) technology has big potential for applications in wireless body area networks (WBANs). The inherent characteristics of UWB signals make them suitable for the wireless interface of medical sensors. In particular, implanted medical wireless sensors for monitoring physiological parameters, automatic drug provision, etc. can benefit greatly from this ultra low power (ULP) interface. As with any other wireless technology, accurate knowledge of the channel is necessary for the proper design of communication systems. Only a few models that describe the radio propagation inside the human body have been published. Moreover, there is no comprehensive UWB in-body propagation model that includes the frequency-dependent attenuation. Hence, this paper extends a statistical model for UWB propagation channels inside the human chest in the 1–6 GHz frequency range by including the frequency-dependent attenuation. This is done by modeling the spectrum shape of distorted pulses at different depths inside the human chest. The distortion of the pulse was obtained through numerical simulations using a voxel representation of the human body. We propose a mathematical expression for the spectrum shape of the distorted pulses that act as a window function to reproduce the effects of frequency-dependent attenuation.**

I. Introduction

In modern telemedicine systems the physiological data of patients can be measured with the aid of electronic sensors located on and inside the human body [1]. The collected medical data is then transmitted wirelessly to an external unit for processing, thereby enhancing the health monitoring, diagnosis, and therapy of the patients. Ultra wideband (UWB) technology has great potential for applications in telemedicine, particularly for medical implant devices, due to its inherent low power consumption, high transmission speed, and simple electronics [2].

In order to design and implement UWB in-body communication systems, accurate knowledge of the propagation channel is necessary. Considerable effort has been devoted to the characterization of the propagation of UWB radio signals for on-body sensors; however, significantly fewer results are reported for the case of UWB implanted devices. The IEEE 802.15.6 standardization group [3] has issued several propagation models for medical and nonmedical devices, both in-body and on-body, for wireless body area networks (WBANs). Nevertheless, the in-body channel models therein characterize narrowband (NB) applications only whereas the UWB models characterize on-body communication channels. To the best of our knowledge, two UWB channel models for implanted sensor communications have been reported in [4], [5] and [6], [7], respectively. The first model characterizes an UWB channel in the 3.4–4.8 GHz frequency band for implanted devices inside the chest within 6–18 mm depth. The second model is more general and covers the 1–6 GHz frequency range for depths up to 120 mm inside the chest.

In order to develop the model in [6], [7] numerical simulations were conducted by using the time-domain finite integration technique (FIT). At different depths inside a voxel representation of the human model [8] that includes tissues dielectric properties [9], several probes were uniformly distributed in the chest region. The channel impulse response (CIR) was extracted using the so-called CLEAN algorithm [10]–[12]. The path loss and time spread for a transmitted pulse through the human tissues can be predicted with this model. Its major drawback, however, is the disregard of the frequency dependent attenuation of the channel for the reproduction of the distorted pulse shape at a given depth for potential applications such as communications and radar. For NB signals the frequency-dependent attenuation can easily be ignored, but over large parts of the spectrum as in the case of UWB signals, it must be considered [10]. This paper aims at improving our own propagation model in [7] through the inclusion of the frequency-dependent attenuation. For this sake we modeled the spectrum shape of transmitted UWB pulses at different depths in order to obtain mathematical expressions for the *window function* that reproduces the frequency-dependent distortion.

The rest of the paper is organized as follows: Section II summarizes the propagation model proposed in [7]. Section III presents the modeling of the frequency-dependent attenuation at different depths inside the chest. Its impact on the signal bandwidth is discussed in Section IV. Section V summarizes our conclusions.

II. Statistical Channel Model

A. Path Loss and Scattering

The *path loss* is a measure of the average attenuation of a signal that propagates from a transmitter to a receiver. The variations around the average value are referred to as *scattering*. These variations are caused by the different

*Research supported by the Research Council of Norway through the MELODY Project (Contract 187857/S10).

A. Khaleghi is with the Intervention Center, Oslo University Hospital, Oslo 0027 Norway, and with the Dept. of Electrical and Computer Engineering, K. N. Toosi University of Technology, Iran (phone: +47-230-70101; fax: +47-230-70110; e-mail: ali.khaleghi@rr-research.no).

R. Chávez-Santiago and I. Balasingham are with the Intervention Center, the Institute for Clinical Medicine, and the Norwegian University of Science and Technology (NTNU), Norway (e-mail: raul.chavez-santiago@rr-research.no; ilangko.balasingham@medisin.uio.no).

material dielectric properties along the propagation path (human chest). The mathematical expression for both path loss and scattering in dB-scale as a function of the depth is given as

$$L_{[\mathrm{dB}]}(d) = L_{0[\mathrm{dB}]} + a(d/d_0)^n + \mathcal{N}(0,\sigma) \qquad (1)$$

where d is the depth from the skin in millimeters ($1 < d < 120$), a is a fitting constant with a value of 0.987, d_0 is the reference depth fixed at 1 mm, L_0 is the loss cross point with a value of 10 dB, and n is an exponent equal to 0.85. The probability density function (PDF) of the scattering (in decibels) is well approximated by a Gaussian distributed random variable (RV), $\mathcal{N}$, with zero mean $\mu = 0$ and standard deviation $\sigma = 7.84$ (See Fig. 1).

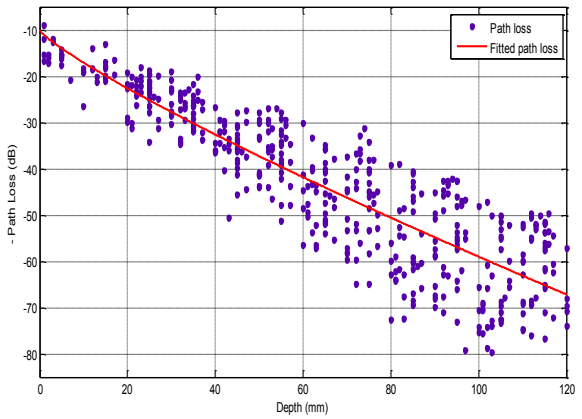

Figure 1. Path loss versus depth inside the human chest [7].

B. Channel Impulse Response

The UWB signal arriving at the receiver can be regarded as the sum of scaled and delayed replicas of the transmitted pulse; hence, the *channel impulse response* (CIR), $h(\tau)$, can be expressed mathematically as

$$h(\tau) = \sum_{k=1}^{N} \alpha_k \delta(\tau - \tau_k) \qquad (2)$$

where α_k and τ_k are the gain and time delay of the k-th multipath component (MPC), respectively, and N is the total number of MPCs. The model in [7] provides the mathematical formulas to reproduce the CIR for two typical depths inside the chest, 20 mm and 80 mm, respectively. Through an extensive simulation campaign it was concluded that $N = 3$ for $d = 20$ mm and $N = 5$ for $d = 80$ mm are sufficient for accurate representation of the channel.

III. Frequency-Dependent Attenuation

After the generation of the CIR by using the model in [7], the reproduction of distorted UWB pulses that propagate through the human chest is possible. However, the model in [7] considers the path loss and dispersive characteristics of the channel and disregards the frequency-dependent distortion of the received pulse. Since the dielectric properties of the human tissues, namely permittivity and conductivity, are frequency dependent [9], the frequency-dependent attenuation over large bandwidths cannot be ignored.

A. Analysis of Pulse Shape

The optimal design of a wireless communication system that operates within a given bandwidth requires estimating the distorted waveform of the pulse after propagation. A straight way to calculate the distorted pulse consists in convoluting the transmitted pulse with the CIR. However, the transmitted pulse in the frequency domain, $P(f)$, must first be shaped by a *window function*, $W(f)$, in order to account for the frequency-dependent loss that it experiences during the propagation through human tissues for a given depth. This can be expressed as

$$\hat{P}(f) = P(f) \cdot W(f) \qquad (3)$$

where $\hat{P}(f)$ is the *shaped pulse* including the frequency-dependent attenuation of the channel. Through electromagnetic (EM) numerical simulations using the scenario described in [7], the frequency-dependent attenuation for different depth intervals in the chest was obtained (Fig. 2). As seen, the frequency-dependent loss varies greatly with depth. When the sensor is implanted deep inside the chest, the frequency-dependent loss of the channel decays more rapidly than near the skin. The decay rate is not linear and this characteristic of the channel has some implications for the selection of the bandwidth and the frequency band that can be used. This will be discussed later in the paper.

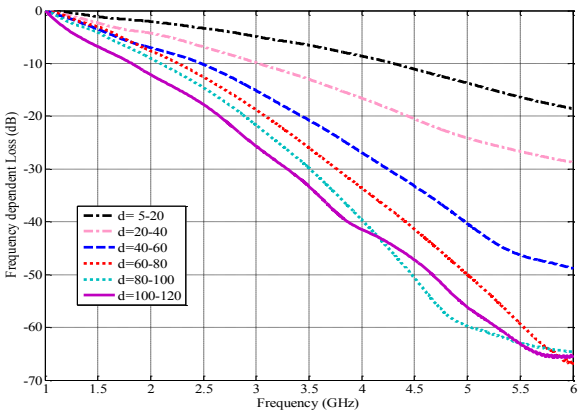

Figure 2. Loss versus frequency for two depths inside the human chest.

B. Frequency- Dependent Attenuation Model

The mathematical model for the decay law of the frequency-dependent loss was obtained by fitting a curve for the interval $5 < d < 20$ mm and $60 < d < 80$ mm in Fig. 2; for simplicity, we refer to these intervals as $d = 20$ mm and $d = 80$ mm, respectively. Similarly to the path loss, the frequency-dependent attenuation (i.e., the window function in the frequency domain) can be represented as

$$W_{[\mathrm{dB}]}(f) = b(f/f_0)^m + c \quad (4)$$

where f_0 = 1 GHz, m is a loss exponent and b, c are fitting constants. The corresponding values of these parameters for d = 20 mm and d = 80 mm are found in Table I.

Notice from Fig. 2 that the decay rate is significantly different between the three curves within $5 < d < 60$ mm; however, for $60 < d < 120$ mm the decay law is roughly the same for all the curves. This effect is caused by the EM wave penetrating from the side and back of the body in addition to the front part of the chest (see the simulation scenario in [7]).

TABLE I. PARAMETERS OF THE FREQUENCY-DEPENDENT LOSS

	m	b	c
d = 20 mm	1.85	–0.71	0.553
d = 80 mm	1.6	–4	4.6

Figure 3(a) shows the spectrum of the second derivative of a Gaussian pulse, which was the transmitted pulse used in the EM numerical simulations in [7]. The shaped spectrum $\hat{P}(f)$ obtained by using (3) and (4) for d = 20 mm and d = 80 mm is also illustrated for each case. The inverse Fourier transform of $\hat{P}(f)$ provides the shaped pulse in the time domain, $\hat{p}(t)$. Figure 3(b) depicts the corresponding pulse shapes $\hat{p}(t)$ for the two different depths together with the second derivative Gaussian pulse in the time domain. Hence, the received signal at a given depth in the time domain, $s(t)$, is calculated as

$$s(t) = \hat{p}(t) * h(t) \quad (5)$$

where $h(t)$ is the unlimited bandwidth CIR given by (2).

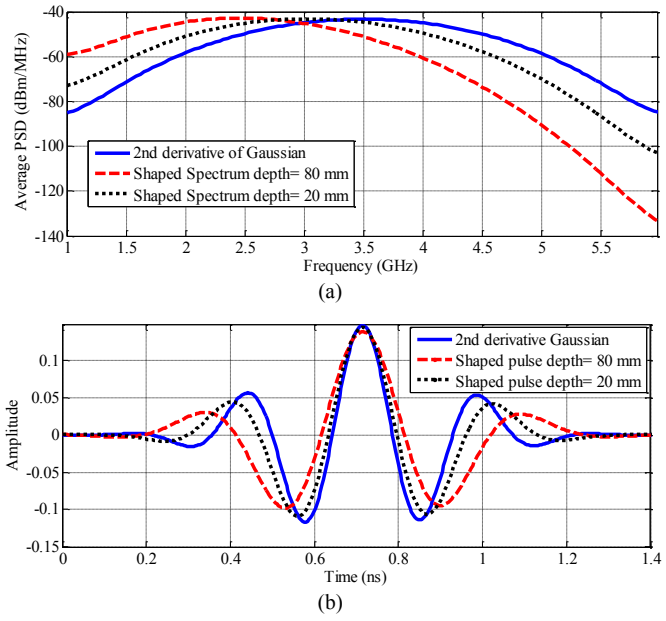

Figure 3. (a) Spectrum of the second derivative Gaussian pulse and the shaped transmitted pulses for two different depths and (b) their corresponding time-domain representation.

C. Implementation and Validation

For the implementation of the channel we used (2) to estimate the CIR, $h(t)$, for d = 20 mm and d = 80 mm, respectively. The amplitude and delay of the MPCs were generated by using the formulas in [7]. For each given depth, 20 channel realizations were generated. The second derivative of a Gaussian pulse (Fig. 3) was the transmitted pulse. The distorted pulses in the time-domain inside the chest were obtained through (5). Figure 4 presents a sample of the distorted pulse for d = 20 mm and d = 80 mm, respectively. The generated channel realizations comply with the average power delay profile and delay spread given in [7]. Figure 5 shows the average power spectral density (PSD) of the 20 channel realizations for the considered depths. As seen, the average PSD is in good agreement with Fig. 3(a). This verified the accuracy of (4). The path loss given by (1) can then be added to scale the received signal power to incorporate the propagation loss and the scattering.

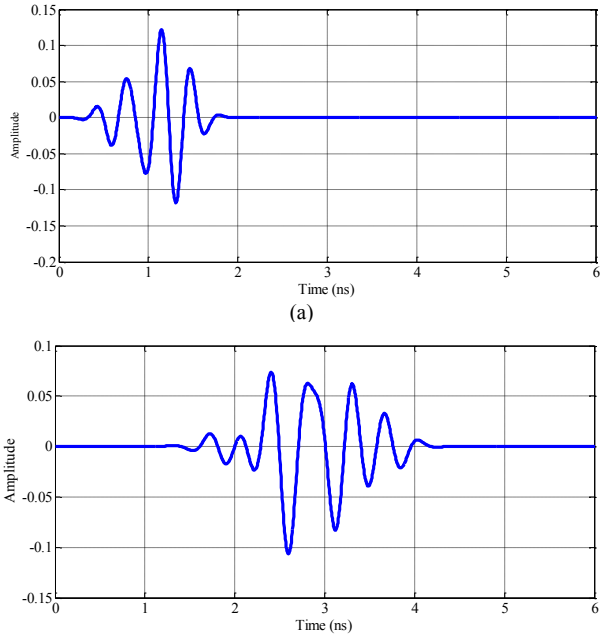

Figure 4. Sample shaped pulse for a depth of (a) 20 mm and (b) 80 mm.

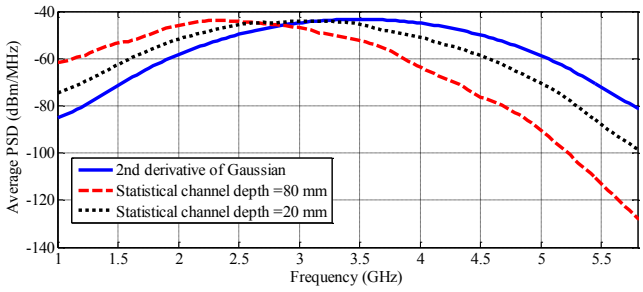

Figure 5. Average power spectral density of 20 realized channels using statistical model and including the frequency dependent loss effect.

IV. DELIMITED BANDWIDTH

The frequency-dependent attenuation has an important implication on the effective bandwidth of the UWB signals. Assume that for a given communication link a maximum level of 10 dB for the frequency-dependent loss can be tolerated. From Fig. 2 it follows that for a depth of $5 < d < 20$ mm a bandwidth of approximately 3.5 GHz (1–4.5 GHz) can guarantee the frequency-dependent loss do not exceed the maximum tolerable level. In contrast, for a deeply implanted sensor between $80 < d < 100$ mm the bandwidth reduces to approximately 1 GHz (1–2 GHz). The calculation of the bandwidth delimited by the frequency-dependent loss is important for the proper design of a communication link. Therefore, we modeled the *delimited bandwidth* by plotting its corresponding values for 10 dB and 15 dB levels of tolerable frequency-dependent loss for the different depths considered in Fig. 2; then, a curve was fitted for each case (Fig. 6). The mathematical expression for the delimited bandwidth in GHz as a function of depth in mm, $BW(d)$, is given as

$$BW(d) = BW_0 \cdot d^{\gamma} \tag{8}$$

where $20 < d < 120$ mm, BW_0 is a reference value, and γ is a decay exponent; the value of these parameters are given in Table II. Note that the delimited bandwidth given by (8) starts at 1 GHz for this case since we considered the frequency band between 1–6 GHz; i.e., the upper frequency of the bandwidth for effective communication is $1 + BW(d)$ GHz.

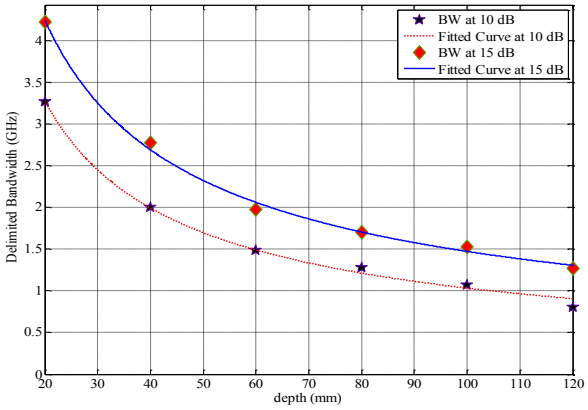

Figure 6. Delimited bandwith as a function of depth in the chest for 10 dB and 15 dB maximum frequency-dependent loss level, respectively.

TABLE II. PARAMETERS OF THE DELIMITED BANDWIDTH

	BW_0	γ
10 dB level	1.85	–0.71
15 dB level	1.6	–4

V. CONCLUSION

In this paper we have extended a statistical model for the attenuation of ultra wideband pulses propagating through the human chest for implanted sensor communications. We included the frequency-dependent attenuation to the available channel model. We obtained the mathematical formula for the frequency-dependent attenuation by analyzing the distorted pulses obtained through numerical simulations. This mathematical expression can be regarded as a window function in the frequency domain that allows modeling the frequency-dependant channel loss accurately. It was observed that the frequency-dependant channel loss varies greatly with depth. Moreover, the bandwidth that an ultra wideband pulse can occupy for effective communication is delimited by the frequency-dependent attenuation too. Therefore, the accurate knowledge of the frequency-dependent channel effects is essential for the proper design of ultra wideband in-body communication links. An interesting topic of research is finding a viable way to extend the delimited bandwidth as much as possible for a fixed depth.

The results presented in this paper are intended to contribute to the better design of implanted communication systems using ultra wideband radio interfaces.

REFERENCES

[1] C. Otto, A. Milenkovic, C. Sanders and E. Jovanov, "System architecture of a wireless body area sensor network for ubiquitous health monitoring," *Journal of Mobile Multimedia*, vol. 1, no. 4, pp. 307–326, 2006.

[2] B. Allen, T. Brown, K. Schwieger, E. Zimmermann, W. Malik, D. Edwards, L. Ouvry and I. Oppermann, "Ultra wideband: Applications, technology and future perspectives," in *Proc. Intl. Workshop on Convergent Technologies (IWCT)*, 2005.

[3] *Channel Model for Body Area Network (BAN)*, IEEE P802.15-08-0780-09-0006, April 27, 2009.

[4] Q. Wang, K. Masami and J. Wang, "Channel modeling and BER performance for wearable and implant UWB body area links on chest," in *Proc. IEEE Intl. Conf. on Ultra-Wideband (ICUWB)*,Vancouver, Canada, September 9–11, 2009, pp. 316–320.

[5] J. Wang and Q. Wang, "Channel modeling and BER performance of an implant UWB body area link," in *Proc. 2nd Intl. Symp. on Applied Sciences in Biomedical and Commun. Technol. (ISABEL)*, Bratislava, Slovak Republic, November 24–27, 2009.

[6] A. Khaleghi, R. Chávez-Santiago, X. Liang, I. Balasingham, V. C. M. Leung and T. A. Ramstad, "On ultra wideband channel modelling for in-body communications," in *Proc. 5th IEEE Intl. Symp. on Wireless Pervasive Computing (ISWPC)*, Modena, Italy, May 5–10, 2010, pp. 140–145.

[7] A. Khaleghi, R. Chávez-Santiago, and I. Balasingham, "Ultra-wideband statistical propagation channel model for implant sensors in the human chest," *IET Microwaves, Antennas & Propagat.*, vol. 5, no. 15, pp. 1805–1812, 2011.

[8] M. J. Ackerman, "Viewpoint: The visible human project," *J. Biocommun.*, vol. 18, no. 2, p. 14, 1991.

[9] C. Gabriel, "Compilation of the dielectric properties of body tissues at RF and microwave frequencies," Brooks Air Force, N.AL/OE-TR-1996-0037, San Antonio, TX, 1996.

[10] A. F. Molisch, "Ultra-wide-band propagation channels," *Proc. IEEE*, vol. 97, no. 2, pp. 353–371, February 2009.

[11] J. A. Hogbom, "Aperture synthesis with a non-regular distribution of interferometer baselines," Astronomy and Astrophysics Supplement, vol. 15, pp. 417–426, 1974.

[12] R. J.-M. Cramer, R. A. Scholtz and M. Z. Win, "Evaluation of an ultra-wide-band propagation channel," *IEEE Trans. Antennas Propagat.*, vol. 50, no.5, pp. 561–570, May 2002.